Rubio,P., Sanz,Y., Rubio,L., Muñoz-Abella,B (2018).Stress Intensity Factor and propagation of an open sickle shaped crack in ashaft under bending. *Theoretical and Applied Fracture Mechanics*, 96, pp.688-698.

DOI: https://doi.org/10.1016/j.tafmec.2017.10.008

Stress Intensity Factor and propagation of an open sickle shaped crack in a shaft under bending

P. Rubio, Y. Sanz, L. Rubio, B. Muñoz-Abella

Department of Mechanical Engineering, University Carlos III of Madrid, Avda. Universidad 30, 28911 Leganés, Madrid, Spain

KEYWORDS

Stress Intensity Factor (SIF)
Cracked shafts
Sickle shaped surface crack SIF expression Propagation of cracks

ABSTRACT

Surface cracks commonly propagate in rotating machines due to cyclic loads. The propagation of these cracks in shafts is an important problem that can lead to catastrophic failure and put lives at risk. Although the majority of the works on cracked shafts consider that the shape of the front of the surface cracks is straight or almond, also sickle-shaped cracks can appear in shafts. In this study, we propose an expression that provides the value of the Stress Intensity Factor (SIF) of an open crack with sickle shape, located at the central section of a shaft, as a function of the relative depth of the crack, the shape factor and the relative position on the crack front. To this end, the SIF along the crack front has been determined through a 3D numerical analysis considering different elliptical geometries of the crack. To validate the expression, we have compared the obtained results with other solutions obtained by numerical approaches of the literature. It has been found that they are in good agreement. Finally, the sickle crack propagation has been analyzed using the expression for sickle cracks proposed and a developed algorithm based on the Paris Law.

1. Introduction

Rotating shafts are commonly used in engineering machines. The structural integrity of these elements can be severely affected by the presence of defects. Working in fatigue, cracks can initiate at the surface and propagate to the inside. If they are undetected, they can grow during the lifetime of the shaft, until a fracture failure occurs, causing irreversible damages.

To analyze the propagation of cracks, it is essential to obtain the Stress Intensity Factor (SIF), which is a parameter that quantifies the stresses at the crack front. The crack shape in shafts can be classified in three groups: straight, almond and sickle. At the beginning, most of the SIF studies considered that the crack front was straight [1 3]. Blackburn [1] and Carpinteri [2] calculated the SIF along the straight front of a crack contained in a shaft under tension by the Finite Element Method (FEM). Valiente [3] obtained the SIF at the central point of a crack with straight front by means of the stiffness derivative method combined with the Finite Element Method. From the results developed a polynomial expression which depends on the crack depth and allows estimating the dimensionless SIF. Later, the studies of the SIF were extended to cracks with almond front. Many works of this kind of shape can be found in the literature [4 17]. In this regard, Mackay and Alperin [4], Forman and Shivacumar [5], and Fonte [6] used fractography techniques to determine the SIF in shafts with almond cracks. They examined with optical and scanning electron microscopes the evolution of the shape of the almond surface cracks and developed a method to obtain the SIF in these cracks under different loading states. Lorentzen et al. [7] proposed a theoretical method to calculate the SIF in these type of cracks by using two and three dimensional photoelasticity experiments with cracked shafts. Also, many authors developed expressions for the SIF of almond cracks. Astiz [8] determined the SIF at the central point of a crack using the stiffness derivative technique to calculate the energy release rate and determined an expression of the SIF as a function of the crack relative depth and the shape factor. Shih y Chen [10] used the numerical model developed by Carpinteri [9] to obtain an expression of the SIF at the central point of the crack and at the ends. Shin and Cai [14] developed a numerical model through the Finite Element Method to determine the SIF in almond cracks under tension and bending and, with the numerical results, made a polynomial fitting dependent on the crack relative depth, the shape factor and the position on the crack front. Rubio et al. [17] developed an expression that provides the SIF value of an almond crack contained in a rotating shaft as a function of the crack relative depth, the location on the crack front, the shape factor and the rotation angle taking into account the crack breathing when the shaft rotates. However, there are a limited number of studies of the SIF, available in the literature, related to sickle shaped cracks [18 23]. Mattheck et al. [18] calculated the SIF at the deepest point of a crack with sickle shape using the Finite

Nomenclature

E	Young's Modulus
ν	Poisson ratio
F	load
L	length of the shaft
D	diameter of the shaft
a	crack depth and minor semi axe of the ellipse of a crack with almond front
a'	minor semi axe of the ellipse of a crack with sickle front
b'	major semi axe of the ellipse of a crack with sickle front
O'	center of the ellipse of a crack with sickle front
α	nondimensional crack depth
β'	nondimensional crack shape for a crack with sickle front
γ	relative position on the crack front
F_I	nondimensional SIF
K_I	Stress Intensity Factor in mode I
K_{ijk}	coefficients of the fitting
σ	maximum bending stress
i	grade of the polynomial in α
j	grade of the polynomial in β'
k	grade of the polynomial in γ
ΔK_I	SIF range
C,m	material constants of the Paris Erdogan law
$\frac{da}{dN}$	crack propagation rate
$\Delta a(P_j)$	advance at any point at the crack front
$\Delta a(A)$	advance at the crack center
$F_I(P_j)$	nondimensional SIF at the different points of the front
$F_I(A)$	nondimensional SIF at the crack center
α_0	nondimensional initial crack depth
β'_0	nondimensional initial crack shape

Element Method and with the results obtained the weight function that can be used for determining the SIF for any other loading case. Carpinteri [21] calculated the values of the SIF at only two points of the crack front of a surface crack with sickle shape in a shaft under bending and tension using a 3D Finite Element Analysis. In other work, Carpinteri [22] determined the SIF at two points of the front of a sickle crack but, in this case, the crack exists at the root of a circumferential notch in a round bar.

After knowing the SIF along the crack front, the fatigue crack growth can be analyzed by means of the Paris Law. Many authors have studied the propagation of almond cracks in shafts [24 30]. Related to the propagation of sickle shaped cracks, a reduced number of studies can be found in the literature. Carpinteri [21] determined the evolution of a sickle crack considering only two points of the front, the central point and the end of the crack. Also, [22] analyzed the growth of a sickle shaped surface crack in a notched round bar under cyclic loading.

In the present work, a polynomial expression of the Stress Intensity Factor of an open sickle shaped surface crack in a shaft has been developed in terms of the geometric parameters of the crack, relative depth and shape factor, and the location on the front, considering a linear elastic behavior of the material. Previously, a numerical analysis has been employed to evaluate the values of the SIF along the front of a sickle surface crack in a shaft. A wide range of crack geometries under pure bending has been considered. The Finite Element code ABAQUS/Standard [31] has been employed for this analysis. The comparison with solutions found in the scientific literature has allowed to validate the SIF expression. Finally, a propagation model for sickle cracks has been developed and the crack front evolution has been analyzed studying how the shape of the sickle crack changes with the growth.

2. Stress Intensity Factor calculation

The values of the SIF along the crack front have been determined by using a 3D Finite Element Analysis. The FEM code ABAQUS/Standard [31] has been used to perform the numerical simulations. A model of a shaft containing a sickle surface crack in its central cross section has been developed. The chosen material for the analysis has been aluminum, with Poisson's coefficient ν, density ρ and Young's modulus Eequal to 0.3, 2800 kg/m^3 and 72 GPa, respectively. The geometrical properties of the shaft are diameter $D = 20$ mm and length $L = 900$ mm. The shaft is subjected to two loads $F = 100$ N located at a distance $d = 225$ mm from the ends of the shaft (see Fig. 1). The finite element mesh used in the calculations is shown in Fig. 2 and consists of approximately 80000 twenty node quadratic isoparametric elements (C3D20 in ABAQUS nomenclature). We have refined the mesh in the vicinity of the crack front.

The transversal section of a shaft that contains a sickle shaped crack is shown in Fig. 3. To describe the front of the crack, we have used an ellipse with semi axes a' and b' whose center is located at point O' (the highest point of that section). The characteristic parameters of this type of cracks are the following:

- $\alpha = \frac{a}{D}$ Crack relative depth.
- $\beta' = \frac{a'}{b'}$ Shape factor of the crack ($\beta' = 0$ corresponds to a crack of straight front and $\beta' = 1$ corresponds to a circular crack).
- $\gamma = \frac{w}{h}$ Relative position on the front.

Eight relative depths have been considered, varying from $\alpha = 0.1$ until $\alpha = 0.8$ in increments of 0.1 (see Fig. 4). Moreover, to find the

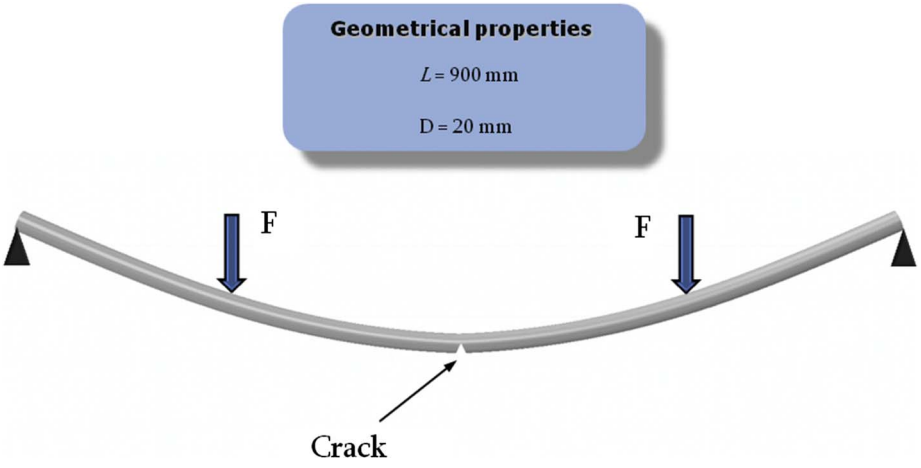

Fig. 1. Geometric model.

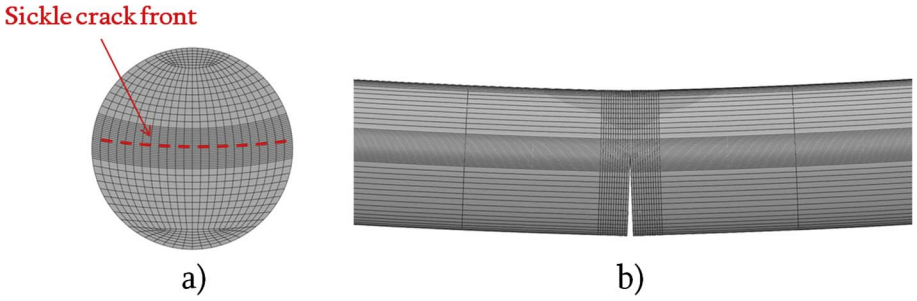

Fig. 2. Mesh of the model. (a) Transversal direction; (b) longitudinal direction.

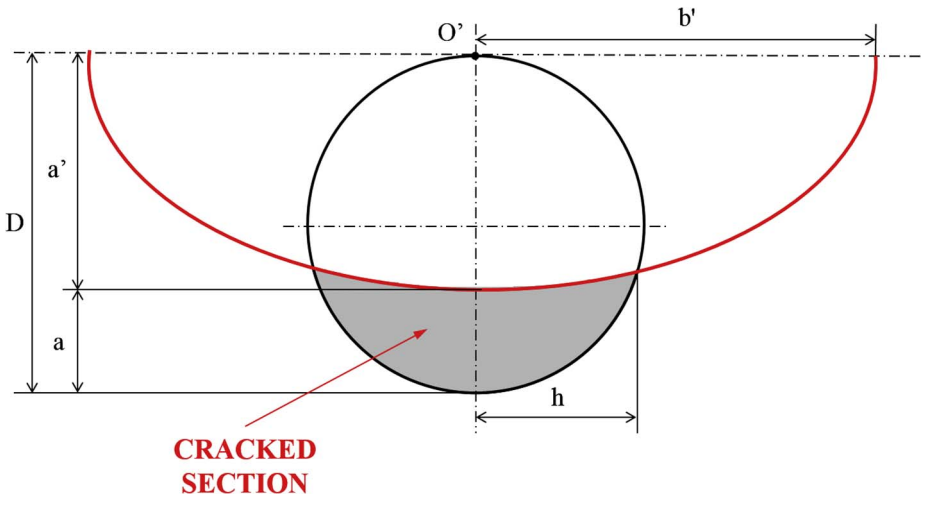

Fig. 3. Characteristic parameters of the elliptical sickle front.

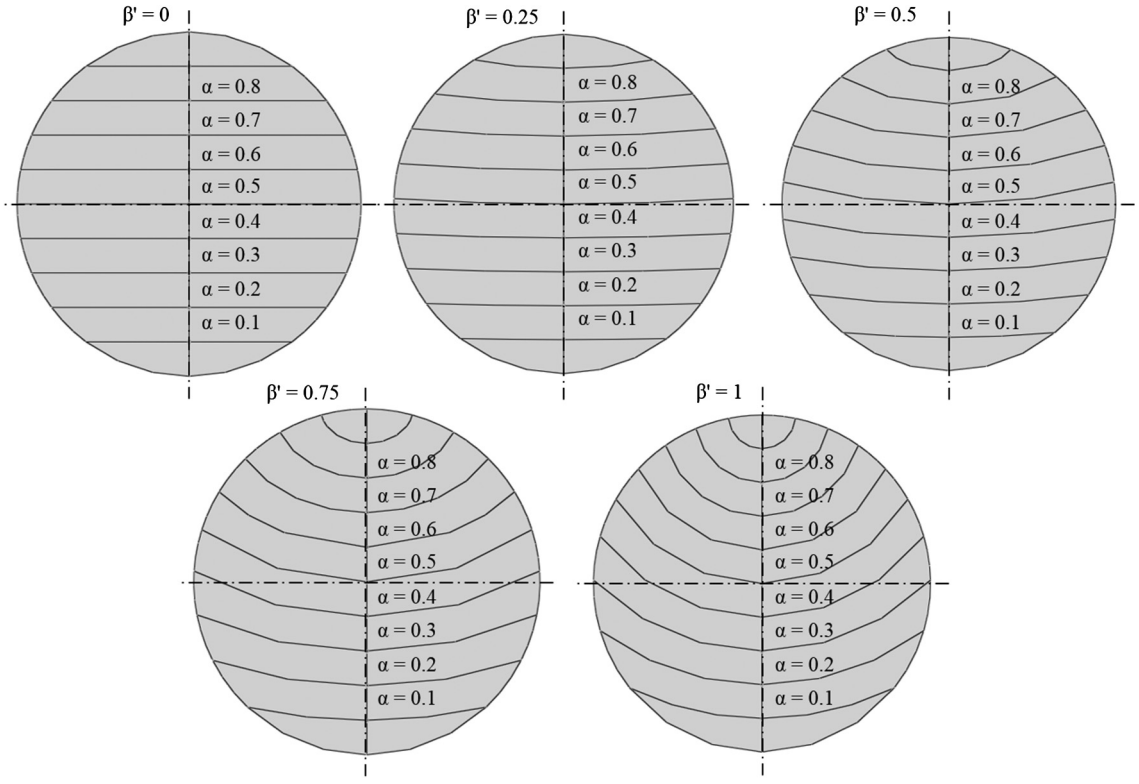

Fig. 4. Different relative depths and shape factors considered.

influence of shape factor β', a range between 0 and 1, with increments of 0.25, has been taken (Fig. 4). Thus, an amount of 40 different models have been made. Finally, the SIF has been determined in eleven relative positions on the front, that go from -0.83 to 0.83 in increments of 0.16. In the study, we have not considered the positions on the front $\gamma = -1$ and 1 due to singularity power at these points depends on the Poisson ratio and on the intersection angle and it is not $-1/2$ [32,9,33,11].

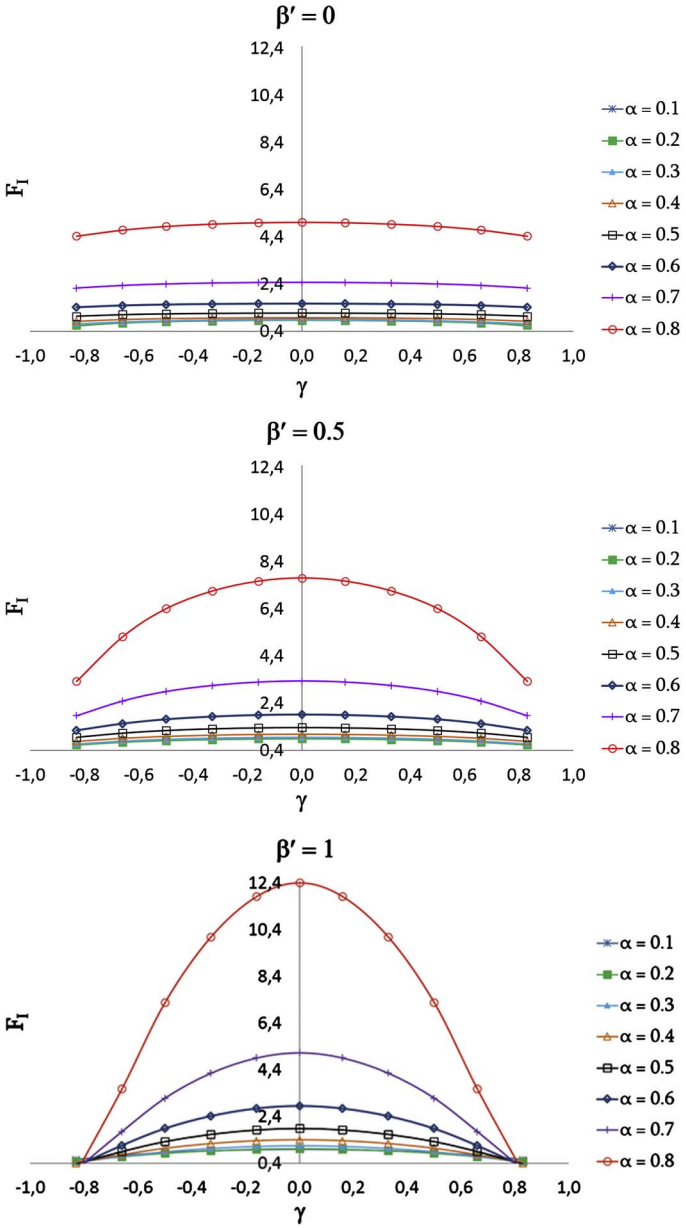

Fig. 5. Nondimensional SIF versus the relative position on the front γ for the different crack depths α and for three crack shapes ($\beta' = 0$; 0.5; and 1).

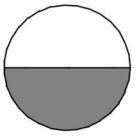

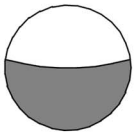

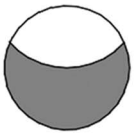

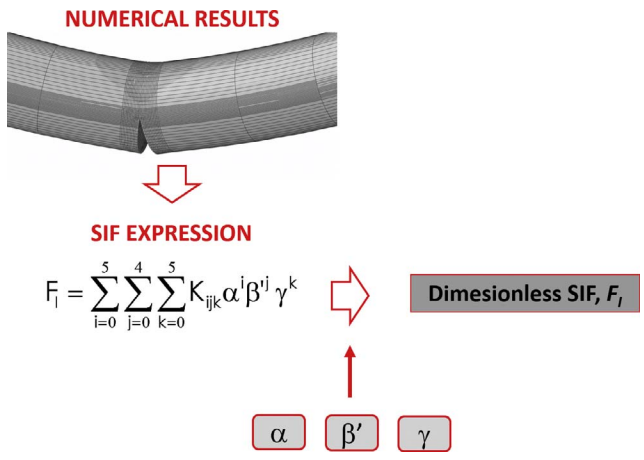

Fig. 6. Procedure to follow to obtain the SIF expression for sickle cracks.

2.1. Results of the SIF

The SIF has been determined for all the considered cases. The dimensionless expression is the following:

$$F_I = \frac{K_I}{\sigma\sqrt{\pi a}} \tag{1}$$

where σ is the maximum bending stress, a is the crack depth, and K_I is SIF in mode I obtained with the numerical study. In Fig. 5 the non dimensional values of the SIF are shown as a function of the relative position on the front γ for the different crack depths α and for three crack shapes ($\beta' = 0$; 0.5; and 1). Looking to the figure, and considering that the results can be extended to other shapes, the following can be concluded:

- The value of the SIF increases with the crack depth α. The stiffness of the shaft decreases as the crack is deeper, due to cracked section is greater.
- All curves of the SIF are symmetrical with respect to the midpoint of the front and convex. The maximum value of SIF is always obtained

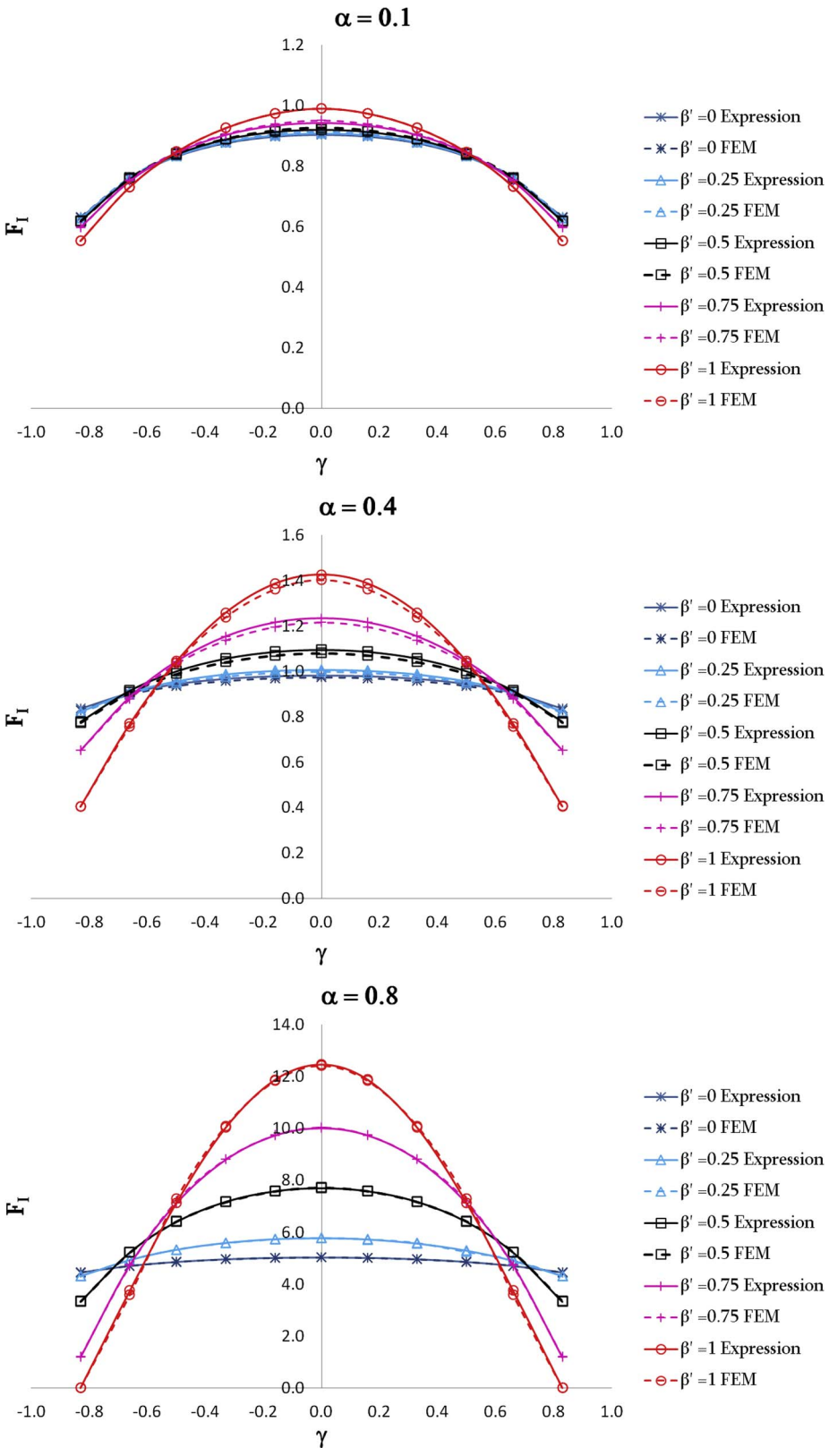

Fig. 7. Comparison among the solutions of the SIF expression and the numerical reference data.

at the center of the crack front, regardless of the crack depth α and the crack shape β'.

- The SIF at the crack center $\gamma = 0$ increases with the crack shape β'. However, the SIF at the crack ends decreases by increasing the shape of the crack β'.

3. The SIF expression for sickle shaped cracks

The determination of an expression that allows obtaining the value of the SIF at every point of the sickle crack front for different crack geometries can be very practical to analyze the propagation of fatigue cracks in shafts. The dimensionless SIF, F_I, under bending can be

Table 1
Mean relative error (%).

	$\beta' = 0$	$\beta' = 0.25$	$\beta' = 0.5$	$\beta' = 0.75$	$\beta' = 1$
$\alpha = 0.1$	0.30	0.29	0.31	0.50	0.67
$\alpha = 0.2$	1.41	1.57	1.59	2.15	2.45
$\alpha = 0.3$	2.44	2.61	2.65	3.53	3.95
$\alpha = 0.4$	0.89	0.91	1.14	1.15	1.33
$\alpha = 0.5$	1.37	1.59	1.27	1.95	2.17
$\alpha = 0.6$	1.60	1.76	1.47	2.10	2.85
$\alpha = 0.7$	0.53	0.57	0.47	0.75	3.84
$\alpha = 0.8$	0.05	0.26	0.11	0.65	1.72

expressed in function of the relative crack depth, the crack shape factor and the relative position on the front:

$$F_I = F_I(\alpha,\beta',\gamma) \tag{2}$$

This expression has been obtained by means of multiple regression techniques and considering all the numerical results obtained in the previous section:

$$F_I = \sum_{i=0}^{5}\sum_{j=0}^{4}\sum_{k=0}^{5} K_{ijk}\alpha^i\beta'^j\gamma^k \tag{3}$$

where i, j and k are the polynomial grades related to the parameters α, β' and γ, respectively, and K_{ijk} are the coefficients of the fitting. The best fitting was obtained with a polynomial of grade 5 in α, grade 4 in β' and grade 5 in γ. A coefficient adjusted $R^2 = 0.9996$ has been obtained. In Tables 2 and 3 of Appendix A, the coefficients K_{ijk} of the fitting are shown. For the time being, no polynomial equation of the SIF for sickle shaped cracks as a function of these parameters has been found in the literature.

In Fig. 6, it can be observed the procedure followed to obtain the SIF expression for sickle cracks.

4. Validation of the SIF expression for sickle shaped cracks

4.1. Comparison with the numerical results

Firstly, with the purpose of checking the goodness of the proposed method, we compare the results obtained using the SIF expression and the numerical model. In Fig. 7, the results obtained with the two procedures have been plotted showing the comparison for three crack depths ($\alpha = 0.1$; 0.4; and 0.8) and all the cases of β'. Although we have chosen these cases for the comparison, the results corresponding to other crack geometries are very similar to the ones that have been exposed. Looking to the figure, it can be observed that there is a great concordance between both results for all the cases. Table 1 shows the MSE (Mean Squared Error) between the results obtained with the expression and the numerical ones for every crack geometry, calculated according to Eq. (4).

$$\bar{\varepsilon}_{F_I}(\%) = 100\frac{1}{n}\sum_{i=1}^{n}\frac{|F_{I,EXP}^{(i)} - F_{I,FEM}^{(i)}|}{F_{I,FEM}^{(i)}} \tag{4}$$

where $F_{I,EXP}$ is the dimensionless SIF obtained with the expression for sickle shaped cracks, and $F_{I,FEM}$ is the dimensionless SIF obtained using the numerical model.

Note that most of the mean squared errors are less 2% and the maximum one is 3.95% showing a great concordance and the goodness of the proposed expression.

4.2. Validation of the SIF expression

4.2.1. Comparison with the numerical results for other crack geometries

Secondly, to validate the SIF expression, the values obtained using the expression have been compared with the numerical data for other crack geometries that have not been used to determine the expression. As an example, two cases, that have been arbitrarily chosen, show the good agreement:

- Case 1: $\alpha = 0.27$ and $\beta' = 0.63$.
- Case 2: $\alpha = 0.61$ and $\beta' = 0.15$.

Fig. 8 shows the comparison between both results. It can be seen a good agreement for the two cases. The MSE are always less than 4.5% for the first case and less than 3% for the second case. For other couple of data (α,β') the result are similar.

4.2.2. Comparison with results obtained from the literature

Finally, a comparison among the solutions of the SIF expression and the results obtained by Carpinteri [21] has been made. Carpinteri [21] calculated the SIF at two points of the front of an open surface crack with sickle shape contained in a shaft under bending using a 3D numerical model and the quarter point displacement technique. Fig. 9 compares the Carpinteri [21] solutions with the current results at the central point of the crack front ($\gamma = 0$). In this case, the SIF has been plotted versus the crack relative depth for the different shape factors. We can see that the results agree very well. We also have obtained the MSE (Mean Squared Error) between both results, according to Eq. (4),

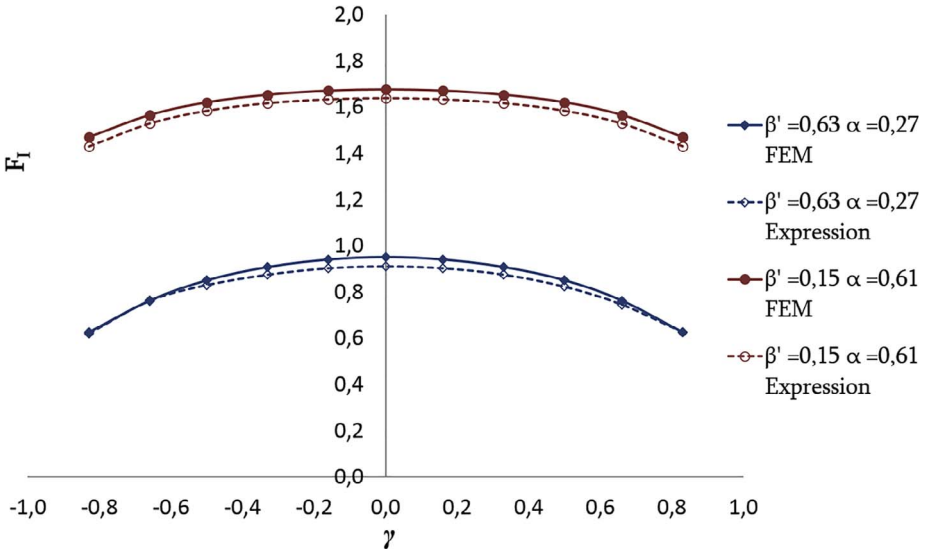

Fig. 8. Comparison with the numerical data for other crack geometries.

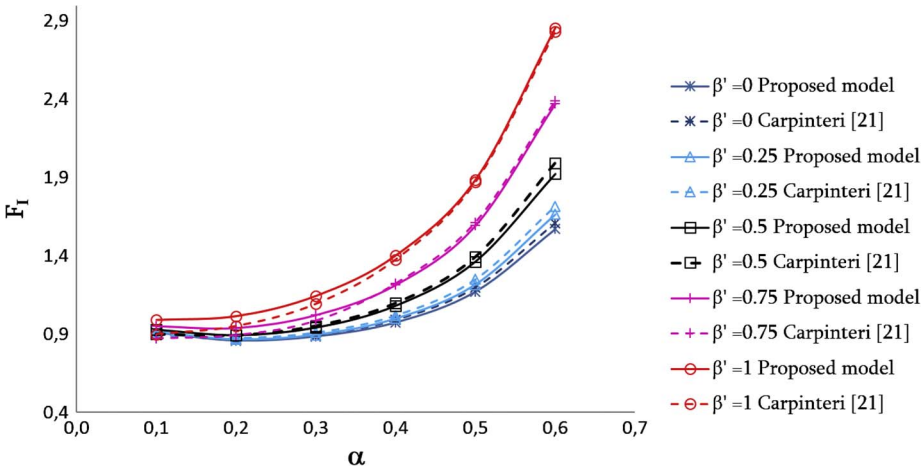

Fig. 9. Comparison among the solutions of the SIF expression and the results obtained by Carpinteri [21] at $\gamma = 0$.

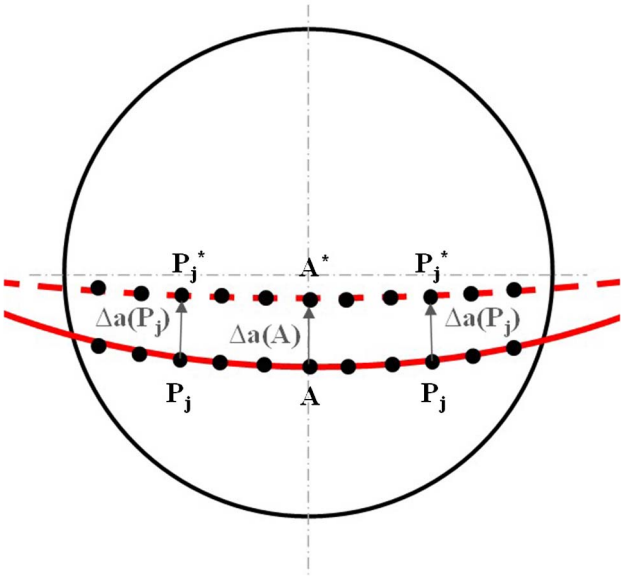

Fig. 10. Fatigue sickle crack growth at each point of the front.

and it is less than 3%. Therefore, these results and the ones obtained at the previous section allow us to validate the SIF expression for sickle shaped cracks.

5. Propagation and crack front evolution for sickle shape cracks

In this section, we have analyzed the crack front evolution for sickle shape cracks until it changes to almond shape using the expression obtained previously. The propagation model for the whole front has been developed to obtain the crack front evolution. This model assumes that, as mentioned before, the crack front has sickle elliptical shape and advances following the Paris Erdogan Law [24,10,11,26,34 36,27]:

$$\frac{da}{dN} = C\Delta K_I^m \tag{5}$$

where ΔK_I is the SIF range; $\frac{da}{dN}$ is the crack propagation rate; C and m are the material constants of the Paris Erdogan Law which are assumed to be $C = 45 \times 10^{-9}$ and $m = 2.9$.

First, the SIF at each point of the front has been calculated using the expression for sickle cracks determined in the previous section. Then, the SIF range at each point has been determined as follows:

$$\Delta K_I = K_{I,max} - K_{I,min} \tag{6}$$

where $K_{I,max}$ is the maximum value of the SIF corresponding to the load $F = 100$ N and $K_{I,min}$ is the minimum value of the SIF corresponding to the load $F = 0$ N. Consequently, the SIF range at the considered point is equal to the maximum value of the SIF, corresponding to the load $F = 100$ N.

We have obtained the crack advance, by integrating the Paris Erdogan Law:

$$\Delta a = \Delta N \cdot C \cdot [\Delta K_I]^m \tag{7}$$

where ΔN is the number of cycles.

The crack depth variation of the point located at the crack center (A) and another point (P_j), are given by the following expressions:

$$\Delta a(A) = \Delta N \cdot C \cdot [\Delta K_I(A)]^m \tag{8}$$

$$\Delta a(P_j) = \Delta N \cdot C \cdot [\Delta K_I(P_j)]^m \tag{9}$$

where j is the number of points along the crack front.

Hence, the crack advance at each point of the crack front $\Delta a(P_j)$ can be expressed as follow:

$$\Delta a(P_j) = \Delta a(A)\left(\frac{\Delta K_I(P_j)}{\Delta K_I(A)}\right)^m \tag{10}$$

where $K_I(P_j)$ is the SIF at the different points of the front; $K_I(A)$ is the SIF at the crack center; and $\Delta a(A)$ is the advance at the crack center that has been given an initial value (see Fig. 10).

Finally, from these points, a new crack front with elliptical sickle shape is fitted using the Least Squared Method. The procedure is repeated iteratively until the depth of the crack reaches a fixed value which has been selected previously in order to finish the propagation study.

As mentioned before, the advance at the crack center $\Delta a(A)$ is given an initial value which remains constant in the whole process. With the purpose of determining the optimum value of this advance at the crack center $\Delta a(A)$, a sensitivity analysis for the $\Delta a(A)$ has been carried out. The results of the sensitivity analysis are shown in Fig. 11. The shape factor β', against the depth α have been plotted for the different values of the crack advance showing the crack front evolution. Two different cases have been represented. In the first case the initial crack depth $\alpha_0 = 0.1$ and initial shape factor $\beta'_0 = 1$ (Fig. 11(a)), and in the second case $\alpha_0 = 0.3$ and $\beta'_0 = 0.75$ (Fig. 11(b)). The values of the crack advance that have been considered are: $\frac{D}{100}$, $\frac{D}{200}$, $\frac{D}{300}$, $\frac{D}{400}$.

We can see that for both cases, the crack front becomes straighter with the growth of the crack, that means that the shape factor decreases progressively until it becomes zero. We can observe that there is a good concordance between the curves corresponding to $\Delta a(A) = \frac{D}{300}$ and $\frac{D}{400}$, so $\Delta a(A) = \frac{D}{300}$ is the value of the advance that has been used in the propagation model.

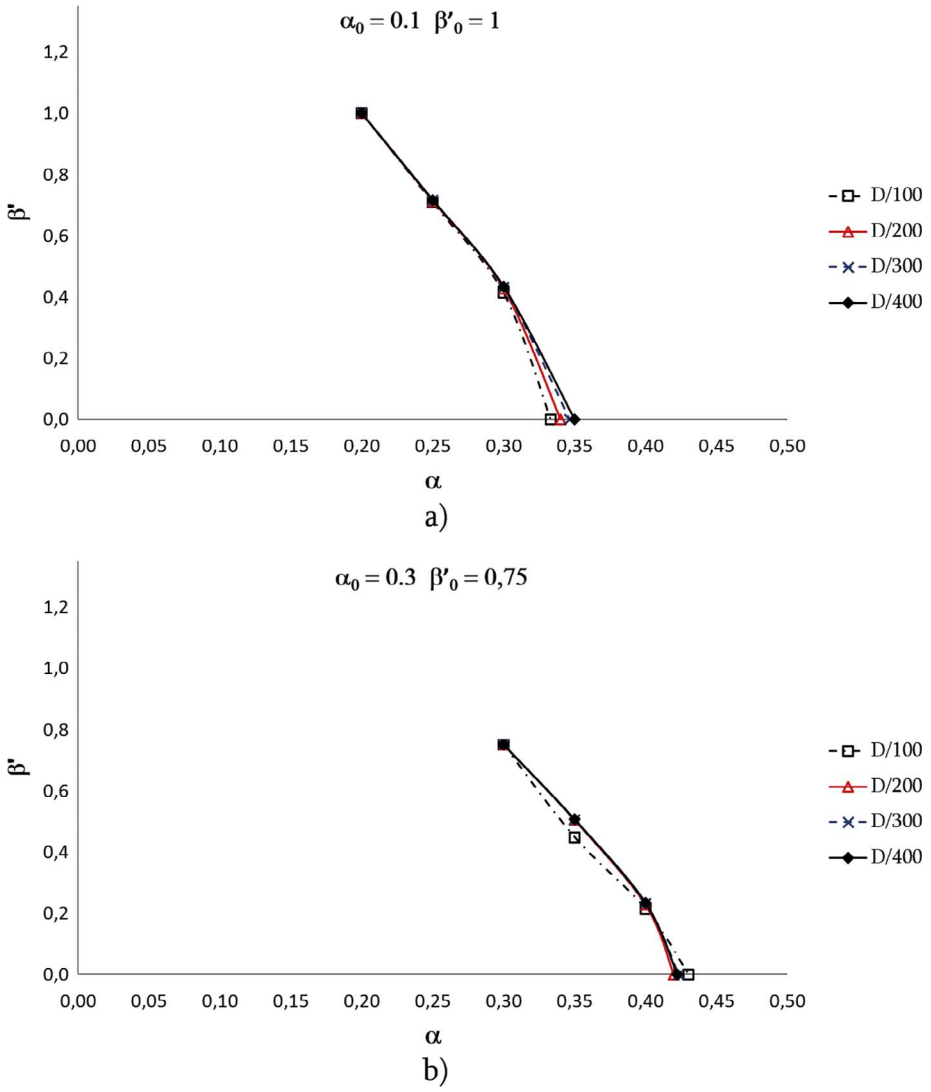

Fig. 11. Sensitivity analysis. (a) $\alpha_0 = 0.1 \quad \beta'_0 = 1$; (b) $\alpha_0 = 0.3 \; \beta'_0 = 0.75$.

5.1. Results of the evolution of the crack front for sickle shape cracks

Fig. 12 shows the evolution of the shape of the sickle crack front that has been obtained by plotting the shape factor β', against the depth α for different initial sickle cracks. The initial crack configurations that have been shown are: initial crack relative depth $\alpha_0 = 0.2$; 0.4; and 0.6, and initial shape factor $\beta'_0 = 0.25$; 0.5; 0.75; and 1. The results corre sponding to other initial crack configurations are analogous to the ones that have been exposed. Note that all the initial sickle cracks tend to become straight with the growth. We can observe that as the initial crack is more circular, it takes longer to become straight. For example, an initial sickle crack of $\alpha_0 = 0.6$ $\beta'_0 = 0.25$ becomes straight when it reaches a depth $\alpha = 0.64$ and an initial sickle crack of $\alpha_0 = 0.6$ $\beta'_0 = 1$ becomes straight when it reaches a depth $\alpha = 0.78$, therefore, this crack takes longer to become straight, that means that the crack is deeper when it becomes straight. Once, the crack adopts the straight shape, as the SIF at the ends of the crack is bigger than the SIF at the center of the crack, the shape will change to almond and the propagation paths should be analyzed with the propagation model [28] developed for almond cracks.

In Fig. 13, the evolution of the front shape of the initial circular cracks ($\beta'_0 = 1$) considered in Fig. 12 is also shown. We can see clearly that regardless of the initial geometry, the front gradually becomes straight with the growth. In addition, the proposed propagation algo rithm also allows studying the number of cycles required to reach a certain depth. The number of cycles required for a circular cracks of $\alpha_o = 0.2$ 0.4; 0.6 to adopt straight shape are $4.3{\cdot}10^5$, $2.9{\cdot}10^5$ and $5.2{\cdot}10^4$ respectively.

6. Conclusions

We have presented an expression to determine the Stress Intensity Factor at any point of the front of a sickle shaped crack contained in a shaft in terms of the geometric parameters of the crack (depth and shape) and the position on the front. To determine this expression, it has been necessary to develop a 3D numerical model of a shaft in bending using The Finite Element code ABAQUS/Standard. The SIF has been determined along the crack front considering different crack geometries. Taking into account all the numerical results, an expression of the SIF has been obtained using multiple regression techniques. The expression of the SIF has been validated comparing the results with the reference numerical data for other crack geometries and with some data of the literature. It can be found that there is a great concordance with all the analyzed cases. It can be concluded that SIF expression seems to be adequate to determine the SIF along the whole crack front for open sickle cracks in shafts and can be used to analyze the propagation of these types of cracks. Finally, the sickle crack propagation has been analyzed using a developed algorithm based on the Paris Law and the expression for sickle cracks proposed. The results obtained with the propagation method indicate that, regardless of the initial geometry,

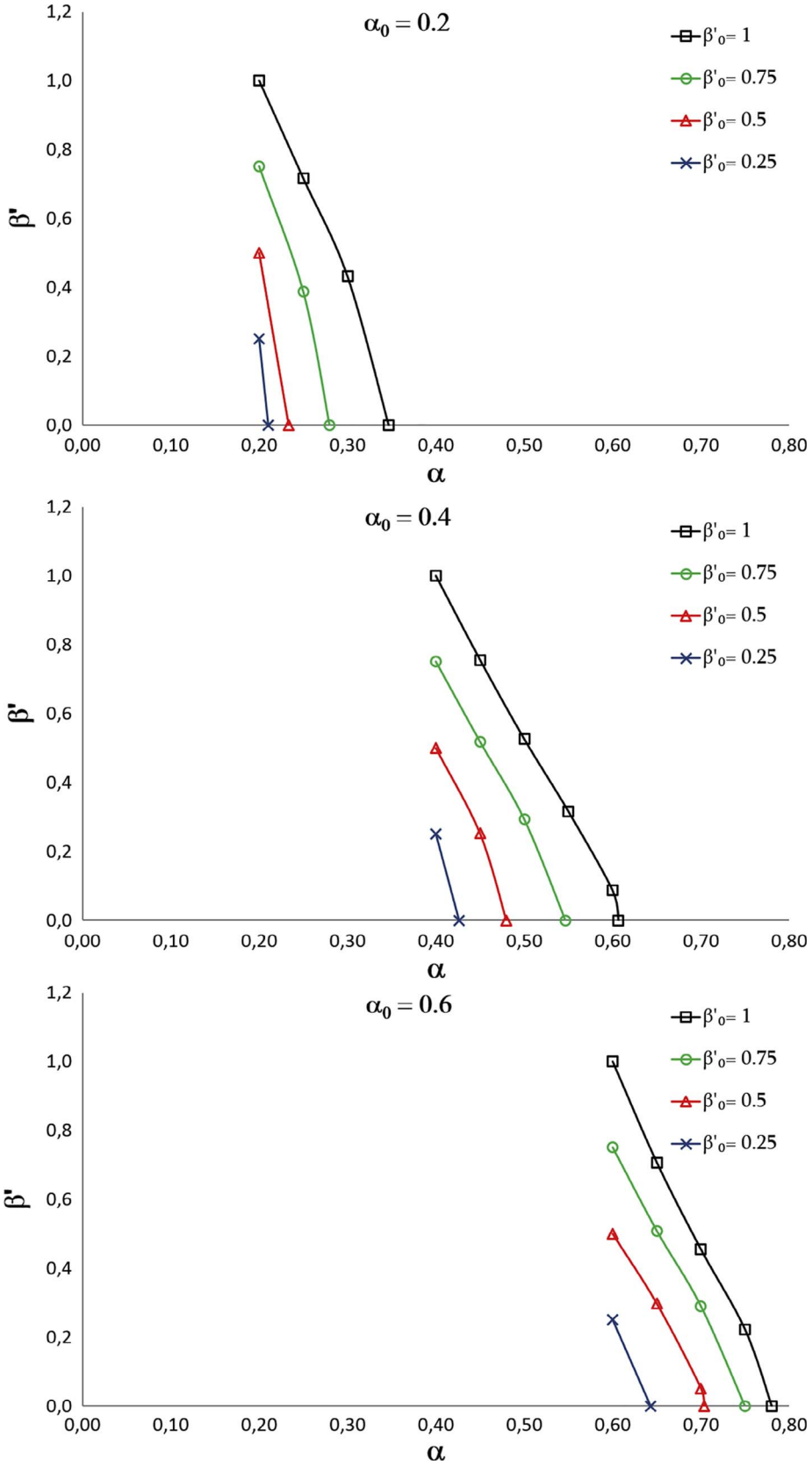

Fig. 12. Factor shape β' against the depth α for different initial shape factors β'_o and for three initial crack depths α_o = 0.2; 0.4; 0.6

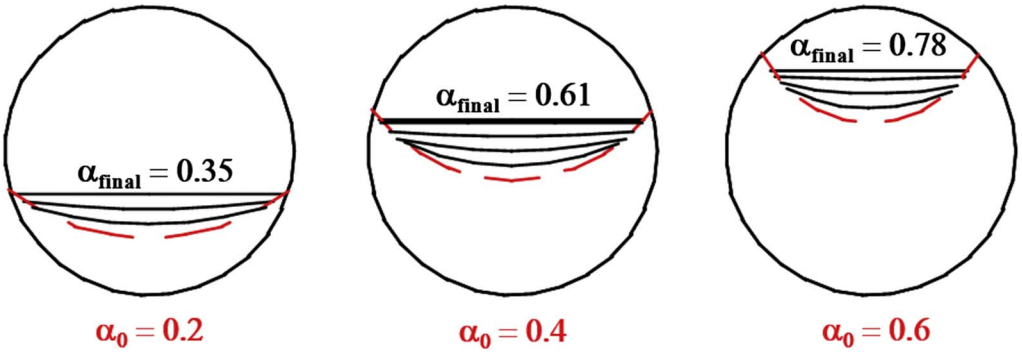

Fig. 13. Evolution of the front shape of the initial circular cracks ($\beta_0' = 1$) for three initial crack depths $\alpha_o = 0.2; 0.4; 0.6$.

Table 2
Coefficients K_{ijk}

i	j	0	1	2	3	4
$k = 0$						
0		0.4875	−0.6294	0.4064	−3.2428	−2.0759
1		9.4830	11.4342	1.9751	50.1501	55.2848
2		−74.6025	−66.0138	−101.7651	−198.8668	164.7026
3		248.3798	153.4645	651.3657	72.5478	−242.4057
4		−365.8062	−142.0032	−1412.5163	692.4108	−48.3627
5		205.5437	37.6398	1000.8080	−754.5669	211.7913
$k = 1$						
0		0.0002	1.4244	−6.1846	8.5633	−3.8024
1		−0.0012	−28.4193	123.4194	−171.0350	76.0250
2		0.0002	192.1328	−834.3504	1156.6009	−514.3335
3		0.0118	−570.5779	2477.4128	−3434.5284	1527.5815
4		−0.0245	763.5559	−3314.7462	4595.2807	−2043.9624
5		0.0145	−375.0129	1627.7396	−2256.4368	1003.6576
$k = 2$						
0		−0.2157	2.4339	−8.1080	14.9954	−5.1173
1		−0.7368	−48.0285	154.4174	−289.8887	94.2611
2		9.4266	326.6910	−1039.5254	1955.5829	−634.2120
3		−32.9586	−976.8284	3006.8426	−5721.0236	1784.8208
4		50.8222	1323.8809	−3905.5388	7553.8428	−2240.8577
5		−29.8109	−664.9542	1848.9177	−3688.0599	1016.0860
$k = 3$						
0		0.0012	−3.7715	16.3692	−22.6579	10.0569
1		−0.0211	74.7819	−324.9914	450.6514	−200.3945
2		0.1275	−500.0042	2173.7802	−3016.3124	1342.2937
3		−0.3414	1461.6847	−6354.7701	8819.6861	−3926.0042
4		0.4165	−1915.3652	8326.0826	−11555.8189	5144.4539
5		−0.1889	914.9745	−3976.7434	5519.0415	−2456.9982
$k = 4$						
0		−0.3794	−4.5817	24.3150	−29.1518	7.2788
1		1.4279	91.0277	−482.5878	569.7931	−132.5685
2		−0.8874	−622.1710	3293.9067	−3841.2626	849.3060
3		−9.4784	1873.6263	−9889.1298	11278.5935	−2255.9302
4		22.1273	−2556.8488	13441.9982	−14891.1075	2556.1960
5		−14.5266	1282.7155	−6701.4332	7070.2149	−869.4949

Table 3
Continued coefficients K_{ijk}

i	j	0	1	2	3	4
$k = 5$						
0		−0.0032	2.3887	−10.3261	14.2595	−6.3171
1		0.0465	−46.9954	204.0124	−282.8193	125.7355
2		−0.2465	309.4811	−1345.7990	1868.6919	−832.0334
3		0.6031	−884.4633	3848.8105	−5347.8440	2382.6944
4		−0.6890	1122.6893	−4886.7860	6792.0216	−3027.0819
5		0.2971	−512.8212	2232.4716	−3103.3668	1383.3587

the sickle crack becomes straight with growth.

Acknowledgements

The authors would like to thank the Spanish *Ministerio de Economía y* Competitividad for the support for this work through the project DPI2013 45406 P.

Appendix A

The coefficients K_{ij} that has been used to determine the SIF expression are the following:
Tables 2 and 3

References

[1] W.S. Blackburn, Calculation of stress intensity factors for straight cracks in grooved and ungrooved shafts, Eng. Fract. Mech. 8 (1976) 731–736.
[2] A. Carpinteri, Stress Intensity Factors for straight- fronted edge cracks in round bars, Eng. Fract. Mech. 42 (1992) 1035–1040.
[3] A. Valiente, Criterios de fractura para alambres, Tesis Doctoral, Universidad Politecnica de Madrid, 1980 (in spanish).
[4] T.L. Mackay, B.J. Alperin, Stress Intensity Factors for fatigue cracking in high-strength bolts, Eng. Fract. Mech. 21 (1985) 391–397.
[5] R.G. Forman, V. Shivakumar, Growth behavior of surface cracks in the circumferential plane of solid and hollow cylinders, in: Fracture Mechanics: Seventeen Volume, ASTM 905, 1986, pp. 59–74.
[6] M.A. Fonte, M.M. Freitas, Semi-elliptical fatigue crack growth under rotating or reversed bending combined with steady torsion, Fatigue Fract. Eng. Mater. Struct. 20 (1997) 895–906.
[7] T. Lorentzen, N.E. Kjaer, T.K. Henriksen, The application of fracture mechanics to surface cracks in shafts, Eng. Fract. Mech. 23 (1986) 1005–1014.
[8] M.A. Astiz, An incompatible singular elastic element for two- and three-dimensional crack problems, Int. J. Fract. 31 (1986) 105–124.
[9] A. Carpinteri, Elliptical-arc surface cracks in round bars, Fatigue Fract. Eng. Mater. 15 (1992) 1141–1153.
[10] Y.S. Shih, J.J. Chen, Analysis of fatigue crack growth on a cracked shaft, Int. J. Fract. 19 (1997) 477–485.
[11] N. Couroneau, J. Royer, Simplified model for the fatigue growth analysis of surface cracks in round bars under mode I, Int. J. Fatigue 20 (1998) 711–718.
[12] A. Levan, J. Royer, Part-circular surface cracks in round bars under tension, bending and twisting, Int. J. Fract. 61 (1993) 71–99.
[13] Y.S. Shih, J.J. Chen, The Stress Intensity Factor study of an elliptical cracked shaft, Nucl. Eng. Des. 214 (2002) 137–145.
[14] C.S. Shin, C.Q. Cai, Experimental and finite element analyses on Stress Intensity Factors of an elliptical surface crack in a circular shaft under tension and bending, Int. J. Fract. 129 (2004) 239–264.
[15] J. Lebahn, H. Heyer, M. Sander, Numerical Stress Intensity Factor calculation in flawed round bars validated by crack propagation tests, Eng. Fract. Mech. 108 (2013) 37–49.
[16] J. Predan, V. Mocilnik, N. Gubeljak, Stress Intensity Factors for circumferential semi-elliptical surface cracks in a hollow cylinder subjected to pure torsion, Eng. Fract. Mech. 105 (2013) 152–168.
[17] P. Rubio, L. Rubio, B. Munoz-Abella, L. Montero, Determination of the stress intensity factor of an elliptical breathing crack in a rotating shaft, Int. J. Fatigue 77 (2015) 216–231.
[18] C. Mattheck, P. Morawietz, D. Munz, Stress Intensity Factors of sickle shaped cracks in cylindrical bars, Int. J. Fatigue 7 (1985) 45–47.
[19] J. Hobbs, R. Burguete, P. Heyes, E. Patterson, A photoelastic analysis of crescent-shaped cracks in bolts, J. Strain Anal. Eng. Des. 36 (2001) 93–99.
[20] A. Carpinteri, R. Brighenti, S. Vantadori, D. Viappiani, Sickle-shaped crack in a round bar under complex mode i loading, Fatigue Fract. Eng. Mater. Struct. 30 (2007) 524–534.
[21] A. Carpinteri, S. Vantadori, Sickle-shaped cracks in metallic round bars under cyclic eccentric axial loading, Int. J. Fatigue 31 (2009) 759–765.
[22] A. Carpinteri, S. Vantadori, Sickle-shaped surface crack in a notched round bar under cyclic tension and bending, Fatigue Fract. Eng. Mater. Struct. 32 (2009) 223–232.
[23] A. Carpinteri, C. Ronchei, S. Vantadori, Stress intensity factors and fatigue growth of surface cracks in notched shells and round bars: two decades of research work, Fatigue Fract. Eng. Mater. Struct. 36 (2013) 1164–1177.
[24] A. Carpinteri, Shape change of surface cracks in round bars under cyclic axial loading, Int. J. Fatigue 15 (1993) 21–26.
[25] A. Carpinteri, Surface flaws in cylindrical shafts under rotary bending, Fatigue Fract. Eng. Mater. 21 (1998) 1027–1035.
[26] X.B. Lin, R.A. Smith, Shape growth simulation of surface cracks in tension fatigued round bars, Int. J. Fatigue 19 (1997) 461–469.
[27] J. Toribio, J.C. Matos, B. Gonzalez, J. Escuadra, Numerical modelling of cracking path in round bars subjected to cyclic tension and bending, Int. J. Fatigue 58 (2014) 20–27.
[28] P. Rubio, Factor de intensidad de tensiones en fisuras elpticas con mecanismo de apertura y cierre en ejes giratorios, Tesis Doctoral, Universidad Carlos III de Madrid, 2014 (in spanish).
[29] M. da Fonte, L. Reis, M. de Freitas, Fatigue crack growth under rotating bending loading on aluminium alloy 7075-t6 and the effect of a steady torsion, Theor. Appl. Fract. Mech. 80 (2015) 57–64.
[30] J. Toribio, J.C. Matos, B. Gonzalez, J. Escuadra, Evolution of crack paths and compliance in round bars under cyclic tension and bending, Theor. Appl. Fract. Mech. 80 (2015) 104–110.
[31] ABAQUS, Abaqus Theory Manual, Version 6.7, in: Dassault Systémes Inc, 2007.
[32] Z.P. Bazant, L.F. Estenssoro, Surface singularity and crack propagation, Int. J. Solids Struct. 15 (1979) 405–426.
[33] A. Carpinteri, R. Brighenti, Part-through cracks in round bars under cyclic combined axial and bending loading, Int. J. Fatigue 18 (1996) 33–39.
[34] X.B. Lin, R.A. Smith, Fatigue growth simulation for cracks in notched and un-notched round bars, Int. J. Mech. Sci. 40 (1998) 405–419.
[35] J. Toribio, J.C. Matos, B. Gonzalez, J. Escuadra, Numerical modelling of crack shape evolution for surface flaws in round bars under tensile loading, Eng. Fail. Anal. 16 (2009) 618–630.
[36] A. Carpinteri, C. Ronchei, S. Vantadori, Fatigue resistant design of round bars weakened by a v-shaped circumferential notch, Proc. Eng. 74 (2014) 321–324.